

Aftershocks halted by static stress shadows

Shinji Toda^{1*}, Ross S. Stein², Gregory C. Beroza³ and David Marsan⁴

Earthquakes impart static and dynamic stress changes to the surrounding crust. Sudden fault slip causes small but permanent—static—stress changes, and passing seismic waves cause large, but brief and oscillatory—dynamic—stress changes. Because both static and dynamic stresses can trigger earthquakes within several rupture dimensions of a mainshock, it has proven difficult to disentangle their contributions to the triggering process^{1–3}. However, only dynamic stress can trigger earthquakes far from the source^{4,5}, and only static stress can create stress shadows, where the stress and thus the seismicity rate in the shadow area drops following an earthquake^{6–9}. Here we calculate the stress imparted by the magnitude 6.1 Joshua Tree and nearby magnitude 7.3 Landers earthquakes that occurred in California in April and June 1992, respectively, and measure seismicity through time. We show that, where the aftershock zone of the first earthquake was subjected to a static stress increase from the second, the seismicity rate jumped. In contrast, where the aftershock zone of the first earthquake fell under the stress shadow of the second and static stress dropped, seismicity shut down. The arrest of seismicity implies that static stress is a requisite element of spatial clustering of large earthquakes and should be a constituent of hazard assessment.

The great 1857 and 1906 San Andreas earthquakes provided the first evidence that stress shadows generated by mainshocks might inhibit subsequent earthquakes^{6,7}. Further studies found that seismicity rates declined for months to years in portions of the stress shadows of the 1983 moment magnitude $M_w = 6.7$ Coalinga, 1989 $M_w = 6.9$ Loma Prieta, 1992 $M_w = 7.3$ Landers, 1994 $M_w = 6.7$ Northridge, 1997 $M_w = 6.1$ Kagoshima, 1999 $M_w = 7.4$ Izmit and 1999 $M_w = 7.6$ Chi-Chi shocks^{8,10,11}, although in some cases there was a seismicity increase at the time of the mainshock, followed by a rate drop beginning days¹², weeks^{10,11,13} or months¹⁴ after the earthquake. Other studies contend that the seismicity rate does not drop in the stress shadows^{1,15–17}. Analyses of large sets of global surface-wave magnitude $M \geq 7$ earthquakes¹⁸ have indicated that ≥ 0.1 bar Coulomb or shear-stress shadows exert only subtle effects on seismicity, and so have not resolved the debate.

At the very least, the conditions under which we can search the seismicity-rate declines in stress shadows have proved to be restrictive. Although the net Coulomb stress change in the crust surrounding an earthquake is zero (Fig. 1a) because there is no energy added to the crust, the net seismicity rate should sharply increase (Fig. 1b). Therefore, when all seismicity within a fixed radial distance from an epicentre or fault is counted, there will be a net gain that obscures any rate drop in the shadows. Detecting rate declines near the fault rupture, where the shadow should be strongest, is hampered by unresolvable geometrical and slip irregularities along the rupture that can produce local stress increases. To measure the rate drop there must also be a high rate

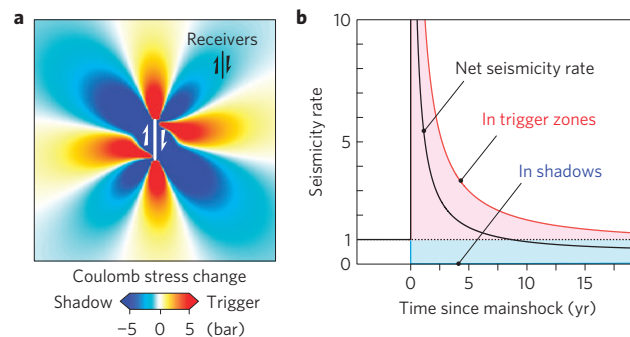


Figure 1 | The stress-trigger/stress-shadow imbalance. **a,b**, Even though there are equal volumes of stress increase and decrease associated with an earthquake (**a**), the resulting seismicity forecast by rate- and state-dependent friction²⁶ yields a sudden rate change followed by a recovery inversely proportional to time, resulting in a net gain in seismicity for times less than about 5 yr (**b**). Here we set the rate/state friction parameter multiplied by the normal stress, $A\sigma$, to 0.4 bar, and aftershock duration, t_a , to 10 yr, values appropriate for the Joshua Tree and Landers earthquakes. At times greater than t_a , the net seismicity rate becomes slightly negative.

of seismicity before the region falls under a stress shadow. The most favourable condition for detection thus occurs when two large nearby but not adjacent mainshocks strike within a few months of each other in a dense seismic network, in which the first earthquake turns on seismicity and the second turns it off⁹.

These requirements are ideally fulfilled by the 23 April 1992 $M_w = 6.1$ Joshua Tree and 28 June 1992 $M_w = 7.3$ Landers earthquakes¹⁹, whose rupture endpoints lie about 13 km apart (black and grey lines in Fig. 2a). The Joshua Tree²⁰ earthquake produced $\sim 6,000$ $M \geq 1.0$ aftershocks within a 20 km radius during the 66 days before the Landers quake struck (blue shocks in Fig. 2a). The four off-fault lobes of the Joshua Tree aftershocks evident in Fig. 1a are well explained by the Coulomb stress imparted by the main rupture²¹. The northern and eastern portions of the Joshua Tree aftershock zone largely shut down after Landers (the rate dropped by 96.5%; blue shocks uncovered by red shocks in Fig. 2a). The portions of the Joshua Tree aftershock zone that were subjected to a stress increase from the Landers earthquake (red stress lobes in Fig. 2b) underwent an abrupt seismicity-rate increase (Fig. 2c), whereas the portion of the aftershock zone that fell under Lander's stress shadow (blue stress lobes in Fig. 2b) shut down beginning 2–3 days later (Fig. 2d).

The Coulomb stress change depends on the source rupture model^{22–25}, and the geometry, rake and friction coefficient of the surrounding 'receiver' faults on which aftershocks occur. The stress lobes shown in Fig. 2, however, are only modestly different for four representative source models (Supplementary Fig. S1), and

¹Disaster Prevention Research Institute, Kyoto University, Kyoto 611-0011, Japan, ²US Geological Survey, Menlo Park, California 94025, USA, ³Department of Geophysics, Stanford University, Stanford, California 94305, USA, ⁴ISTerre, Université de Savoie, CNRS, 73376 Le Bourget du Lac, France.

*e-mail: toda@rcep.dpri.kyoto-u.ac.jp.

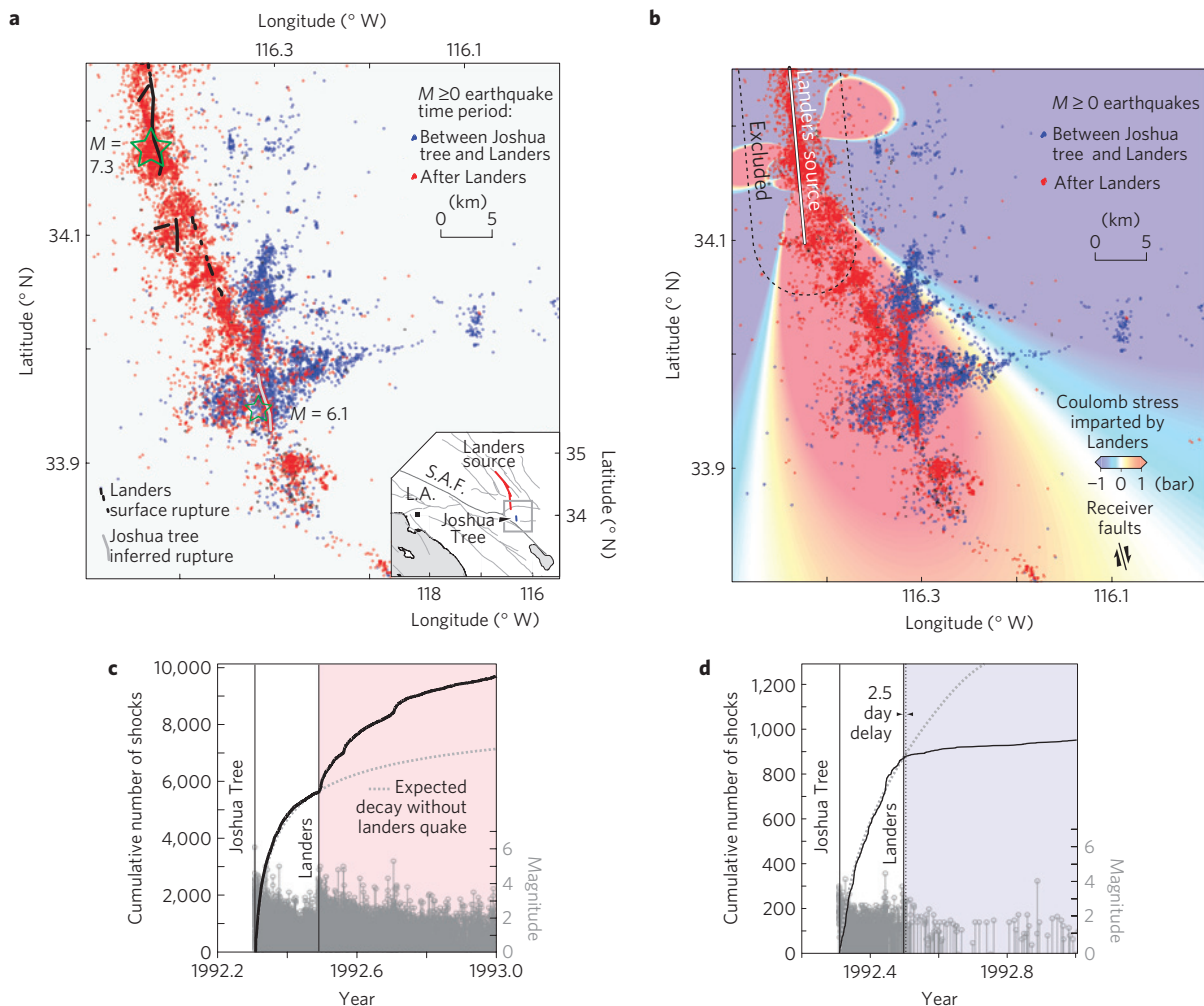


Figure 2 | Seismicity shutdown in the Landers stress shadow. **a**, Seismicity (SHKL, ref. 33, relocated catalogue without quarry blasts) associated with the 1992 Joshua Tree and Landers earthquakes. Earthquakes occurring during the 66 days between the Joshua Tree and Landers earthquakes are blue, and earthquakes from Landers to the end of 1992 (184 days) are red, revealing a shutdown within the stress shadow (blue region). The San Andreas Fault (S.A.F.) and Los Angeles (L.A.) are shown in the inset. **b**, Coulomb stress imparted by the Landers earthquake at 7.5 km depth for vertical right-lateral receiver faults striking 345° with friction of 0.4. **c,d**, Time series of earthquakes in the stress-trigger (**c**) and stress-shadow (**d**) zones. Earthquakes within 5 km of the Landers source (dashed line in **b**) are excluded because of source-model simplicity and uncertainty.

values of receiver fault friction (Supplementary Fig. S2). The most common Joshua Tree aftershocks are right lateral, followed by normal mechanisms (a full presentation of the mechanisms with ternary diagrams of their diversity is shown in Supplementary Fig. S3). Observed $M \geq 2$ earthquakes in the calculated stress shadows for both strike-slip and normal receivers declined after the Landers earthquake regardless of assumed friction (Supplementary Fig. S4). In Fig. 3, the stress imparted by the Landers earthquake²² to the nodal planes of the focal mechanisms is shown, rather than that to a fixed receiver fault geometry as in Fig. 2. There is a mean 2 bar stress drop on the nodal planes, but with some planes being subjected to a stress increase (Fig. 3b). Because of mechanism uncertainty and because we do not know which nodal plane slipped, the histogram of the Fig. 3b inset is only a realization of the true distribution, but it is probably more realistic than using the single, dominant receiver plane for all shocks of Fig. 2b.

Is the seismicity-rate drop real? The rate drop cannot be attributed to a detection artefact, as the seismic network coverage was uniform across the Joshua Tree aftershock zone throughout 1992 (the station distribution is shown in Supplementary Fig. S5, and the magnitude of completeness as a function of time and space is shown in Supplementary Fig. S6). Further, because the

shadow is located the same distance from the Landers rupture as the trigger zone, no detection bias favours the shadow, and both have the same seismic station density (Supplementary Fig. S5). The seismicity-rate decline is evident across all magnitude bands (Supplementary Fig. S7), and is clear even when the immediate post-mainshock periods are excluded. If detection rather than the seismicity rate had decreased, the rate decrease would have appeared in both trigger and shadow zones, which is not observed. We might ask if the shutdown is seen only because the Landers earthquake ruptured largely northward, away from Joshua Tree, resulting in negligible dynamic stress, but the peak dynamic stress at the site of the shutdown is calculated to be 45–60 bar¹⁵, dwarfing the 2 bar static stress drop. Similar dynamic stress is calculated in the trigger zone¹⁵, where the seismicity rate jumped. Finally, the seismicity-rate increase in the trigger zone makes it unlikely that the shutdown occurred because the Joshua Tree aftershocks had already expended the potential earthquake-nucleation sites.

Either a sudden or delayed shutdown can be explained by a rate/state friction implementation of Coulomb stress transfer²⁶. Using the observed background seismicity rate, fitting for the aftershock duration, t_a , and a constitutive parameter multiplied by the normal stress, $A\sigma$, and using only the calculated stress decreases

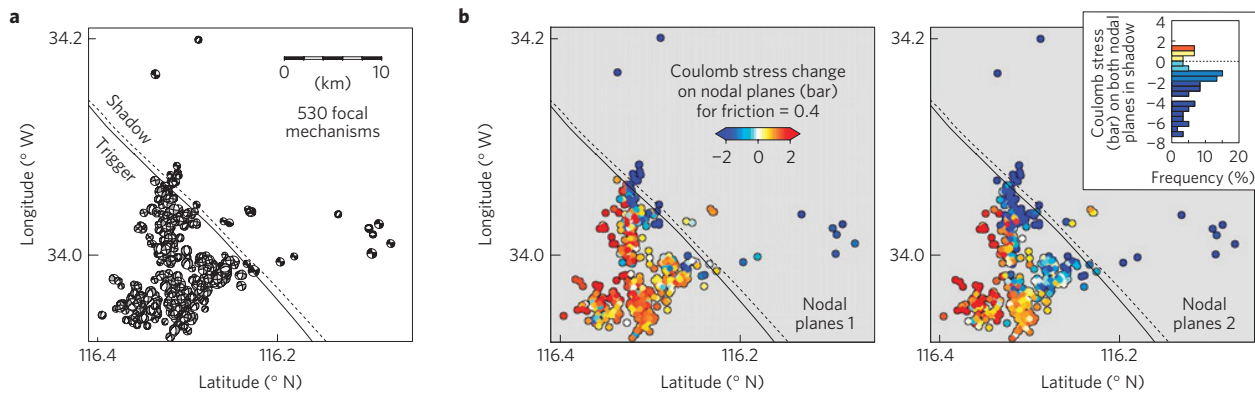


Figure 3 | Stress shadow imparted to the nodal planes of Joshua Tree aftershocks. a, Focal mechanisms for $M \geq 2.0$ events during the 66 days between the Joshua Tree³² and Landers earthquakes. The black mechanisms lie within the stress shadow for strike-slip (dashed) and normal (solid) receiver faults. **b**, For non-zero fault friction, the Coulomb stress is different on the two planes, and so we calculate it on both planes using a standard Landers source model²². The stress decreases on most, but not all, mechanisms. Inset: histogram of Coulomb stress changes for both nodal planes within the stress shadow (northeast of the solid line).

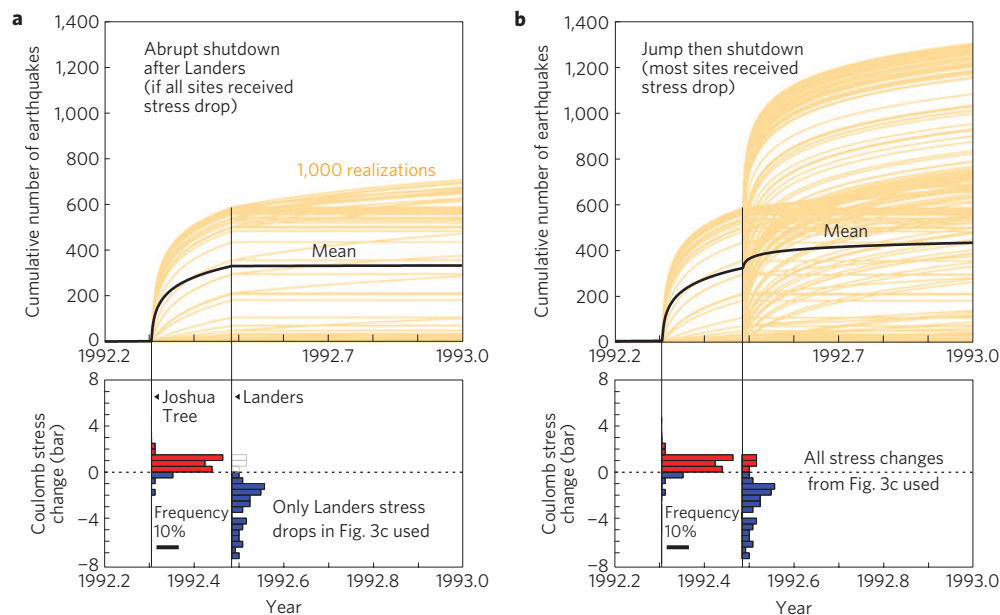


Figure 4 | Explanation of immediate and delayed rate drops in the stress shadow. Calculation of the expected number of Joshua Tree aftershocks in the Landers stress shadow. The Coulomb stress changes for the Joshua Tree and Landers earthquakes are drawn at random from the distribution shown in the lower panels. The seismicity-rate equation²⁶ is evolved for the Joshua Tree and Landers earthquakes in daily steps. The black curve is the mean of all 1,000 time histories (tan curves). **a**, When only the Landers stress decreases are used, the rate drop is immediate. **b**, When the full range of inferred stress changes imparted by Landers to the aftershock focal mechanisms is used, there is a rate jump and a delayed decline.

from Fig. 3c, a sudden shutdown of seismicity would have occurred (Fig. 4a). The same parameters can be employed to match the immediate seismicity-rate increase in the trigger zone, using the calculated stress increases to its aftershocks. However, when the full range of the calculated stress changes in Fig. 3c is used instead, a rate jump followed by a delayed shutdown occurs (Fig. 4b). This can explain the observed delay, as well as the one-day⁹ to three-month¹⁴ delay in the rate drop for other earthquakes (Methods). It is also possible that an immediate rate jump could be the product of dynamic stress triggering.

The more diverse the geometry of the faults surrounding the mainshock, the more likely there will be an immediate rate increase followed by a delayed decrease. Fault diversity most probably results from a low or heterogeneous regional tectonic stress^{27,28}. Other sources of heterogeneity in the stress-change distribution can also delay the seismicity shutdown, including variations in

crustal lithology or fluid pressure, the stress imparted by nearby aftershocks, or a recent change in the tectonic stress, none of which we consider. On the source fault itself, slip heterogeneity adds to this diversity, which may explain why delays are often observed in stress shadows along the fault rupture²⁶.

We have designed this study to overcome the shortcomings and limitations of our analysis of a seismicity-rate drop in the stress shadow of the 1997 Kagoshima, Japan, doublet⁹. First, several authors objected to the use of arbitrary boxes to search for rate drops^{12,16}. Here, we define the sampled area by the stress changes themselves rather than by boxes, and the resulting seismicity-rate drop is observed over an area four times larger than at Kagoshima. A second criticism was that the seismicity-rate drop might instead be an artefact caused by degraded earthquake detection after the mainshock, or a change in background rate beforehand^{12,16,19,29,30}. Here, we fully explore the network detection level and completeness

magnitude in time and space, and can exclude these possibilities. Third, some argued that, as seismicity-rate drops in stress shadows are commonly delayed, Kagoshima is exceptional rather than representative²⁹. Here the shutdown delay is short, so there is little doubt that the Landers earthquake caused it, but long enough to be observable and thus part of a continuum that extends to longer delays. Finally, we consider that the Kagoshima study inadequately explored model uncertainty. Here we used four source models rather than one and three values of friction rather than two, and calculated the stress changes not only on the two dominant receiver planes but also on all aftershock nodal planes.

We thus find that stress shadows of large mainshocks can indeed halt aftershock occurrence, as required by the static Coulomb triggering hypothesis. The occurrence of a seismicity-rate drop in the stress shadow does not mean that dynamic triggering cannot also occur. Instead, we argue that static stress triggering must be one source of the production of aftershocks, and by extension subsequent mainshocks.

Methods

In Fig. 2b, the dominant strike of right-lateral receiver fault planes is determined from the 464 observed focal mechanisms within the stress shadow, calculated under the condition that the rake is within 10° of pure right lateral (Supplementary Fig. S4a). The same calculation is made for normal faults (Supplementary Fig. S4b), which comprise the next most common mechanism. The consequences of these assumptions, as well as those for the full range of possible fault friction (0.0–0.8), are shown in Supplementary Fig. S4c–f.

In Fig. 3, stress is calculated on both nodal planes of each mechanism at its hypocentre, rather than at a fixed depth as in Fig. 2b–d. We do not assume we know which nodal plane slipped, and so the stress changes on both planes are included in the histogram. Only if fault friction were zero would the Coulomb stress change have been the same on both planes.

In Fig. 4, the background seismicity rate in the stress shadow is set to $12 M \geq 2.0$ earthquakes yr^{-1} , on the basis of the 1 January 1984–11 April 1992 catalogue. The distribution of Coulomb stress changes for the Joshua Tree and Landers earthquakes are simulated by 1,000 Monte Carlo draws from the distributions of Joshua stress changes. They are then evolved in one-day time steps until the time of the Landers earthquake, at which time they are modified by draws from the distributions of Landers stress changes, and again evolved in one-day time steps until 1993. The fitted rate and state friction parameters are $A\sigma = 0.1$ bar and $t_0 = 10$ yr. This aftershock duration is similar to that for the 1992 $M_w = 6.1$ Big Bear aftershock sequence located at the same distance from the San Andreas fault³¹ as Joshua Tree.

Received 23 August 2011; accepted 5 April 2012; published online 6 May 2012

References

- Kilb, D., Gomberg, J. & Bodin, P. Earthquake triggering by dynamic stresses. *Nature* **408**, 570–574 (2000).
- Freed, A. M. Earthquake triggering by static, dynamic, and postseismic stress transfer. *Annu. Rev. Earth Planet. Sci.* **33**, 335–367 (2005).
- Hill, D. P. & Prejean, S. G. in *Treatise on Geophysics* Vol. 4 (ed. Kanamori, H.) 257–291 (Elsevier, 2007).
- Gomberg, J. & Johnson, P. Dynamic triggering of earthquakes. *Nature* **437**, 830 (2005).
- Velasco, A. A., Hernandez, S., Parsons, T. & Pankow, K. Global ubiquity of dynamic earthquake triggering. *Nature Geosci.* **1**, 375–379 (2008).
- Jaumé, S. C. & Sykes, L. R. Evolution of moderate seismicity in the San Francisco Bay region, 1850 to 1993: Seismicity changes related to the occurrence of large and great earthquakes. *J. Geophys. Res.* **101**, 765–789 (1996).
- Harris, R. A. & Simpson, R. W. In the shadow of 1857—the effect of the great Ft. Tejon earthquake on subsequent earthquakes in southern California. *Geophys. Res. Lett.* **23**, 229–232 (1996).
- Stein, R. S. The role of stress transfer in earthquake occurrence. *Nature* **402**, 605–609 (1999).
- Toda, S. & Stein, R. S. Toggling of seismicity by the 1997 Kagoshima earthquake couplet: A demonstration of time-dependent stress transfer. *J. Geophys. Res.* **109**, B02303 (2003).
- Wyss, M. & Wiemer, S. The change in the probability for earthquakes in southern California due to the Landers Magnitude 7.3 earthquake. *Science* **290**, 1334–1338 (2000).
- Toda, S. & Stein, R. S. Response of the San Andreas fault to the 1983 Coalinga–Nuñez Earthquakes: An application of interaction-based probabilities for Parkfield. *J. Geophys. Res.* **107**, 2126 (2002).

- Woessner, J., Hauksson, E., Wiemer, S. & Neukomm, S. The 1997 Kagoshima (Japan) earthquake doublet: A quantitative analysis of aftershock rate changes. *Geophys. Res. Lett.* **31**, L03605 (2004).
- Daniel, G., Marsan, D. & Bouchon, M. Perturbation of the Izmit earthquake aftershock decaying activity following the 1992 M_w 7.2 Düzce, Turkey earthquake. *J. Geophys. Res.* **111**, B05310 (2006).
- Ma, K.-F., Chan, C.-H. & Stein, R. S. Response of seismicity to Coulomb stress triggers and shadows of the 1999 $M_w = 7.6$ Chi-Chi, Taiwan, earthquake. *J. Geophys. Res.* **110**, B05S19 (2005).
- Kilb, D. A strong correlation between induced peak dynamic Coulomb stress change from the 1992 M7.3 Landers, California, earthquake and the hypocenter of the 1999 M7.1 Hector Mine, California earthquake. *J. Geophys. Res.* **108**, 2012 (2003).
- Felzer, K. R. & Brodsky, E. E. Testing the stress shadow hypothesis. *J. Geophys. Res.* **110**, B05S09 (2005).
- Mallman, E. P. & Zoback, M. D. Assessing elastic Coulomb stress transfer models using seismicity rates in southern California and southwestern Japan. *J. Geophys. Res.* **112**, B03304 (2007).
- Mallman, E. P. & Parsons, T. A Global search for stress shadows. *J. Geophys. Res.* **113**, B12304 (2008).
- Marsan, D. & Nalbant, S. Methods for measuring seismicity rate changes: A review and a study of how the M_w 7.3 Landers earthquake affected the aftershock sequence of the M_w 6.1 Joshua Tree earthquake. *Pure Appl. Geophys.* **162**, 1151–1185 (2005).
- Savage, J. C., Lisowski, M. & Murray, M. Deformation from 1973 through 1991 in the epicentral area of the 1992 Landers, California, earthquake ($M_s = 7.5$). *J. Geophys. Res.* **98**, 19951–19958 (1993).
- King, G. C. P., Stein, R. S. & Lin, J. Static stress changes and the triggering of earthquakes. *Bull. Seismol. Soc. Am.* **84**, 935–953 (1994).
- Wald, D. J. & Heaton, T. H. Spatial and temporal distribution of slip for the 1992 Landers, California earthquake. *Bull. Seismol. Soc. Am.* **84**, 668–691 (1994).
- Cohee, B. P. & Beroza, G. C. Slip distribution of the 1992 Landers earthquake and its implications for earthquake source mechanics. *Bull. Seismol. Soc. Am.* **84**, 692–712 (1994).
- Cotton, F. & Campillo, M. Frequency domain inversion of strong motions: Application to the 1992 Landers earthquake. *J. Geophys. Res.* **100**, 3961–3975 (1995).
- Hernandez, B., Cotton, F. & Campillo, M. Contribution of radar interferometry to a two-step inversion of the kinematic process of the 1992 Landers earthquake. *J. Geophys. Res.* **104**, 13083–13099 (1999).
- Dieterich, J. A constitutive law for rate of earthquake production and its application to earthquake clustering. *J. Geophys. Res.* **99**, 2601–2618 (1994).
- Marsan, D. Triggering of seismicity at short timescales following Californian earthquakes. *J. Geophys. Res.* **108**, 2266 (2003).
- Marsan, D. Can coseismic stress variability suppress seismicity shadows? Insights from a rate-and-state friction model. *J. Geophys. Res.* **111**, B06305 (2006).
- Stacy, S., Gomberg, J. & Cocco, M. Introduction to special section: Stress transfer, earthquake triggering, and time-dependent seismic hazard. *J. Geophys. Res.* **110**, B05S01 (2005).
- Cocco, M. *et al.* Sensitivity study of forecasted aftershock seismicity based on Coulomb stress calculation and rate- and state-dependent frictional response. *J. Geophys. Res.* **115**, B05307 (2010).
- Toda, S., Stein, R. S., Richards-Dinger, K. & Bozkurt, S. Forecasting the evolution of seismicity in southern California: Animations built on earthquake stress transfer. *J. Geophys. Res.* **110**, B05S16 (2005).
- Hardebeck, J. L. & Shearer, P. M. Using S/P amplitude ratios to constrain the focal mechanisms of small earthquakes. *Bull. Seismol. Soc. Am.* **93**, 2434–2444 (2003).
- Shearer, P., Hauksson, E. & Lin, G. Southern California hypocenter relocation with waveform cross-correlation, Part 2: Results using source-specific station terms and cluster analysis. *Bull. Seismol. Soc. Am.* **95**, 904–915 (2005).

Acknowledgements

We thank D. Kilb, A. Michael, T. Parsons, R. Harris and D. Schorlemmer for guidance and reviews.

Author contributions

All authors contributed to the ideas and tests pursued in the analysis. G.C.B. discovered the data set and its implications, S.T. designed and carried out most of the calculations, D.M. enhanced the statistical rigour and explained the delayed-shutdown phenomenon and R.S.S. wrote most of the text.

Additional information

The authors declare no competing financial interests. Supplementary information accompanies this paper on www.nature.com/naturegeoscience. Reprints and permissions information is available online at www.nature.com/reprints. Correspondence and requests for materials should be addressed to S.T.